The Scheimpflug condition

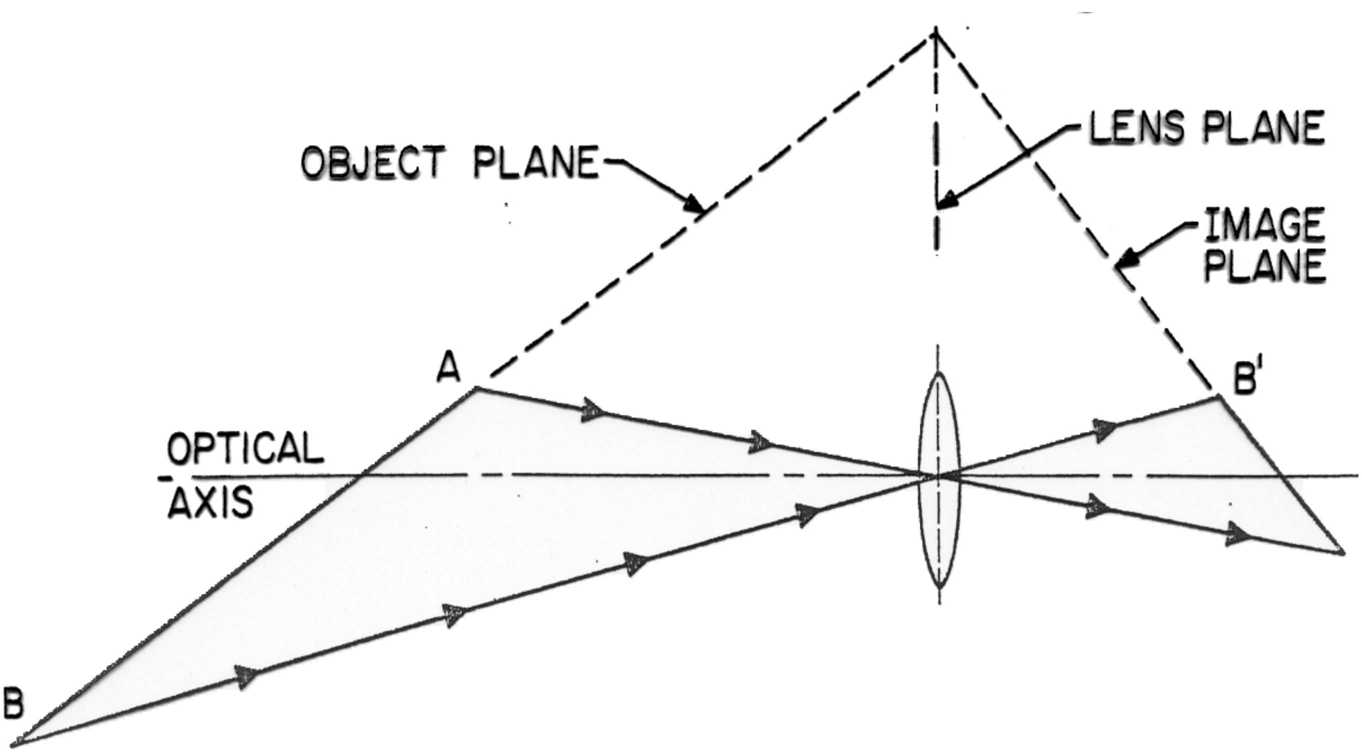

The object plane and the image plane intersect at right angles at the plane of the lens.

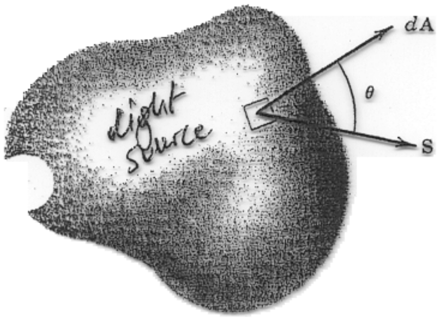

Radiometry

$$\Phi_e = \left(\begin{array}{c}\text{rate at which}\\ \text{energy is radiated}\\ \text{away from the source}\end{array}\right) = \frac{d\left(\begin{array}{c}\text{radiant}\\ \text{energy}\end{array}\right)}{d\,(\text{time})}$$

Fig. 4.9 Closed surface used for calculating the total radiant flux.

Radiant flux: $\Phi_e = \oiint \vec{S}\cdot d\vec{A}$ [Watts]

$d\vec{A}$ ← differential surface area element vector

Radiant energy flux density $\vec{S}$ $\left[\frac{\text{Watts}}{\text{cm}^2}\right]$

↑ aka Poynting vector

$$\Phi_e = \oiint \left[\int \frac{dS}{d\Omega}\cos\theta\, d\Omega\right] dA$$

$$L_e = \frac{dS}{d\Omega} \quad \left[\frac{\text{Watts}}{\text{cm}^2\cdot\text{sterrad}}\right]$$

radiance

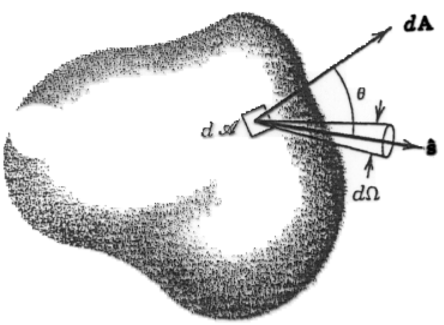

Fig. 4.10 Geometry for the radiant flux integral in the case where the light possesses a range of directions.

$$L_e = \frac{dS}{d\Omega} = \frac{d^2\Phi_e}{\cos\theta\, d\Omega\, dA} \Rightarrow d^2\Phi_e = L_e \cos\theta\, d\Omega\, dA$$

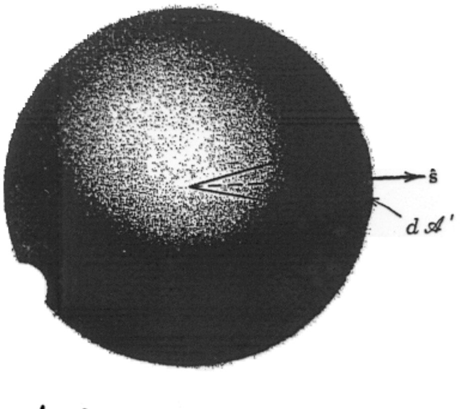

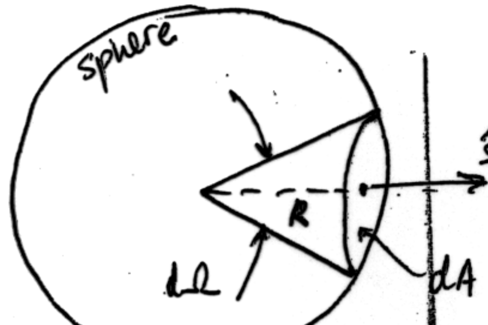

Fig. 4.11 Defining relationships for the solid-angle differential element.

solid angle element:

$$d\Omega = \frac{dA}{R^2}$$

10/5/00
wk5-6-4

{source} radiant exitance $M_e \left[\frac{\text{Watts}}{\text{cm}^2}\right]$: $d\Phi_e = M_e\, dA$

{detector} irradiance $E_e \left[\frac{\text{Watts}}{\text{cm}^2}\right]$: $d\Phi_e = E_e\, dA$

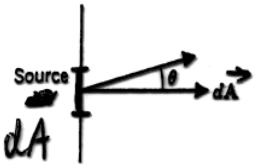

Fig. 4.14 The radiant exitance is the power per unit area leaving $d\mathscr{A}$ and going to the right. It includes all propagation directions θ from 0 to 90°.

$$d\Phi_e = \int_{(1/2)} d^2\phi_e = dA \underbrace{\int_{(1/2)} L_e \cos\theta\, d\Omega}_{\text{radiant exitance}} \Rightarrow M_e = \int_{(1/2)} L_e \cos\theta\, d\Omega$$

one-half of full (4π) solid angle, i.e. outward from the source surface

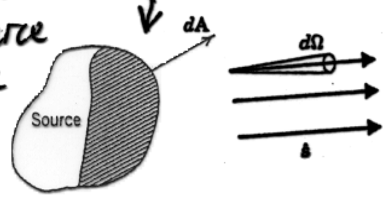

Fig. 4.15 The radiant intensity $I(\hat{s})$ represents the total power per unit solid angle radiating in direction $\hat{s}$ from a finite source.

Radiant intensity: $I_e = \frac{d\Phi_e}{d\Omega} \left[\frac{\text{Watts}}{\text{sterrad}}\right]$

$$d\Phi_e = \int d^2\Phi_e = d\Omega \underbrace{\iint L_e \cos\theta\, dA}_{\text{radiant intensity}} \Rightarrow I_e = \iint L_e \cos\theta\, dA$$

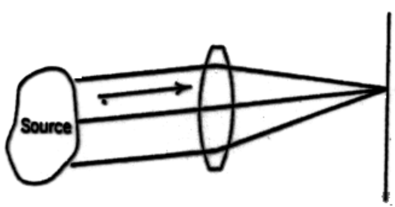

← I_e = observable !

Fig. 4.16 All rays in the same direction $\hat{s}$ are focused at the same point by the lens.

10/5/00
wk5-b-5

Lambertian source: equivalent to small hole in cavity

The light distribution at the hole

- uniform across the hole aperture
- propagates in all directions with equal radiance

For a Lambertian source,

$$M_e = \int_{(1/2)} L_e \cos\theta \, d\Omega = L_e \int_{(1/2)} \cos\theta \, d\Omega$$

(L_e ↑ does not depend on direction!)

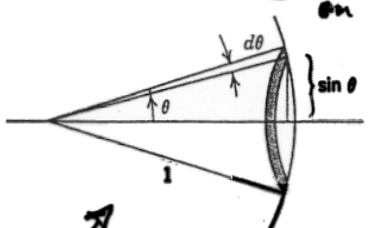

Fig. 4.18 Annular solid angle differential element.

define $d\Omega$ such that $\cos\theta = \text{constant}$ over $d\Omega$

$$d\Omega = \underbrace{2\pi \sin\theta}_{\text{annular length}} \; \underset{\uparrow \text{ annular thickness}}{d\theta}$$

$$M_{e,\text{Lambertian}} = L_e \int_0^{\pi/2} \cos\theta \left(2\pi \sin\theta\right) d\theta$$

$$= \pi L_e \int_0^{\pi/2} d\left(\sin^2\theta\right)$$

$$= \pi L_e$$

10/5/00
wk5-b-6

ABERRATIONS

- Deviation of the wavefront from its "ideal" spherical shape due to imperfect refraction by the optical elements

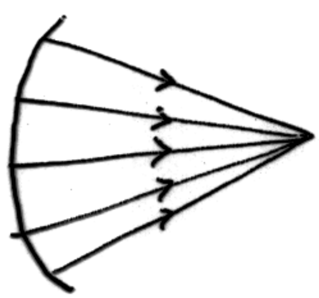

perfect spherical wavefront (focuses to a point)

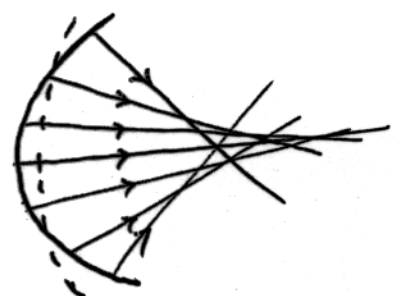

aberrated wavefront does not come to a focus → image is blurred

Optical elements (lenses, mirrors) produce perfect (non-aberrated) wavefronts only in the paraxial approximation (i.e., for angles of propagation near the optical axis).
At larger angles, 5 kinds of aberrations (called "Seidel" aberrations) occur

PRIMARY (SEIDEL) ABERRATION

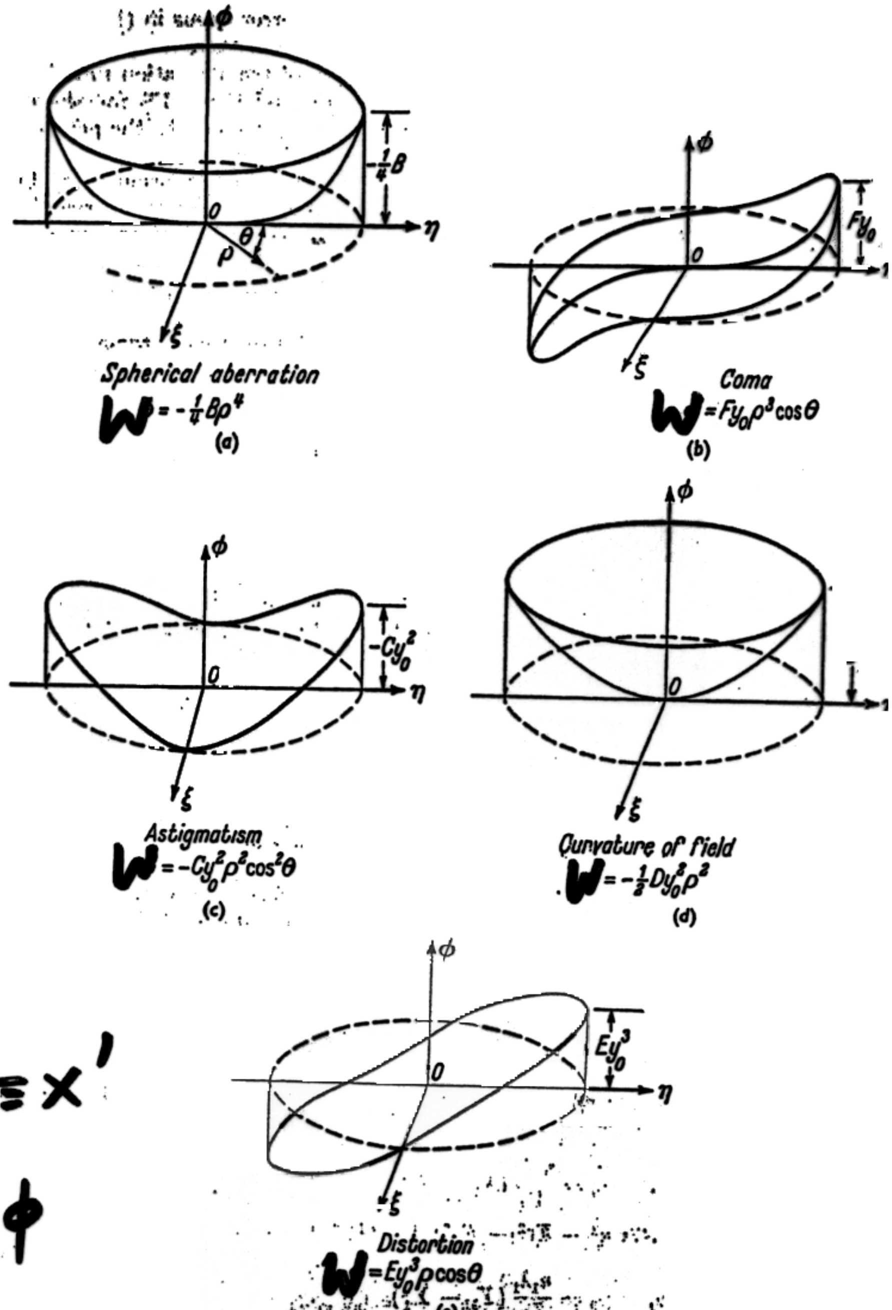

$y_0 \equiv x'$

$\theta \equiv \phi$

Fig. 5.3. The primary wave aberrations.

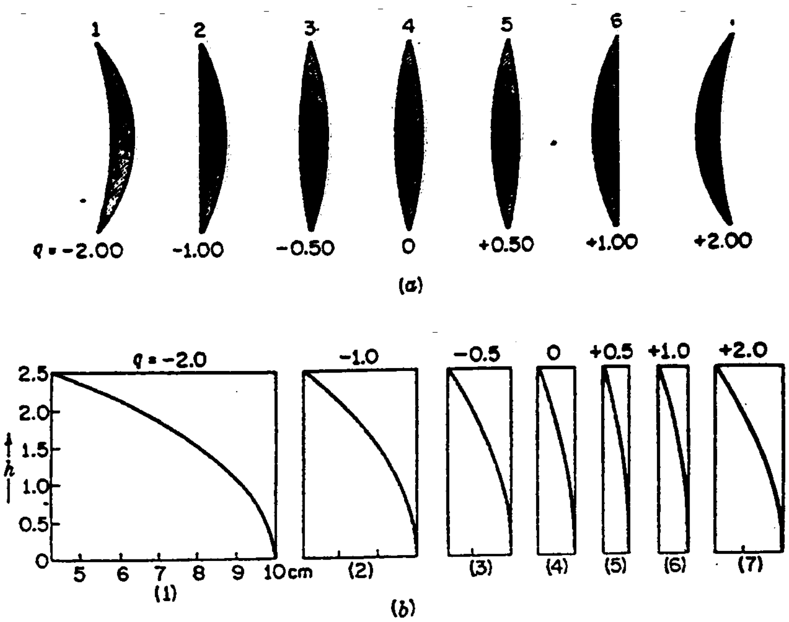

FIGURE 9F
(*a*) Lenses of different shapes but with the same power or focal length. The difference is one of bending. (*b*) Focal length versus ray height *h* for these lenses.

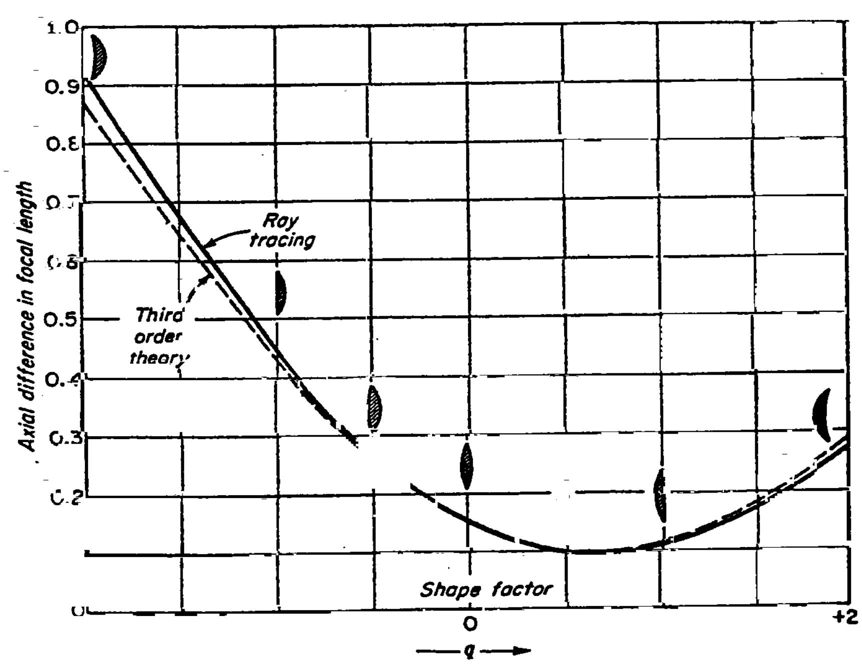

FIGURE 9G
... for lenses of different shape but the same

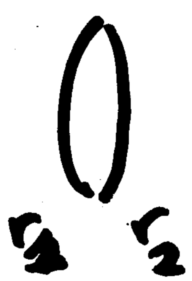

thin lens

$$q = \frac{r_2 + r_1}{r_2 - r_1}$$

$$\frac{1}{s} + \frac{1}{s'} = (n-1)\left(\frac{1}{r_1} - \frac{1}{r_2}\right) = \frac{1}{f}$$

$$p = \frac{s' - s}{s' + s}$$

$$s = \frac{2f}{1+p} \qquad s' = \frac{2f}{1-p} \qquad r_1 = \frac{2f(n-1)}{q+1}$$

$$r = \frac{2f(n-1)}{\ }$$

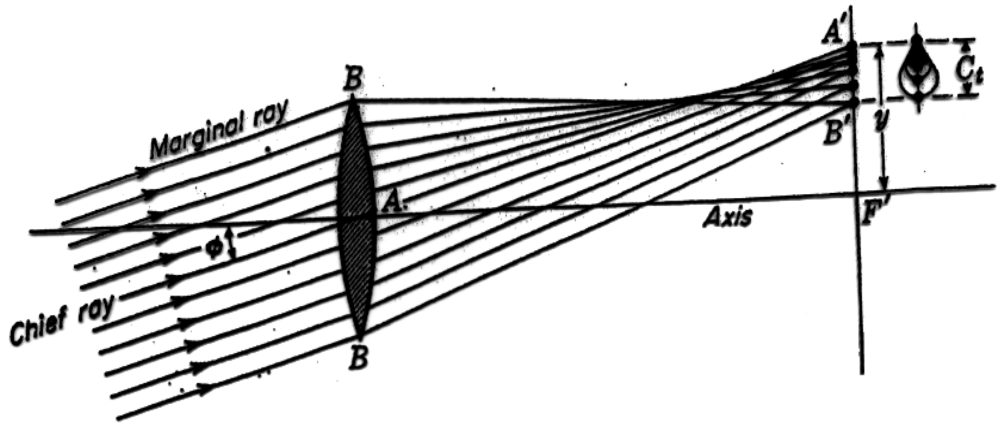

FIGURE 9I
Coma, the second of the five monochromatic aberrations of a lens. Only the tangential fan of rays is shown.

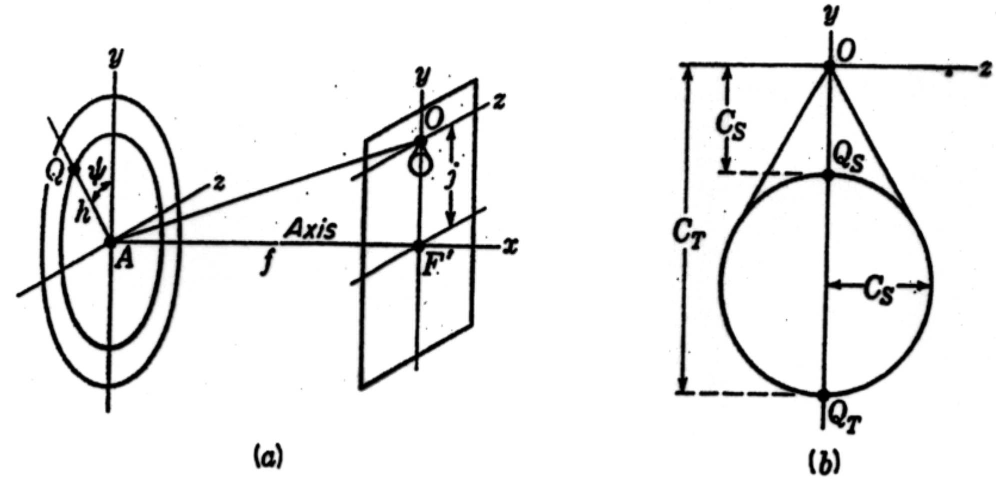

FIGURE 9K
Geometry of coma, showing the relative magnitudes of sagittal and tangential magnifications.

$$C_T = 3 C_s$$

equation of comatic figure

$$y = C_s (2 + \cos 2\psi)$$

$$z = C_s \sin 2\psi$$

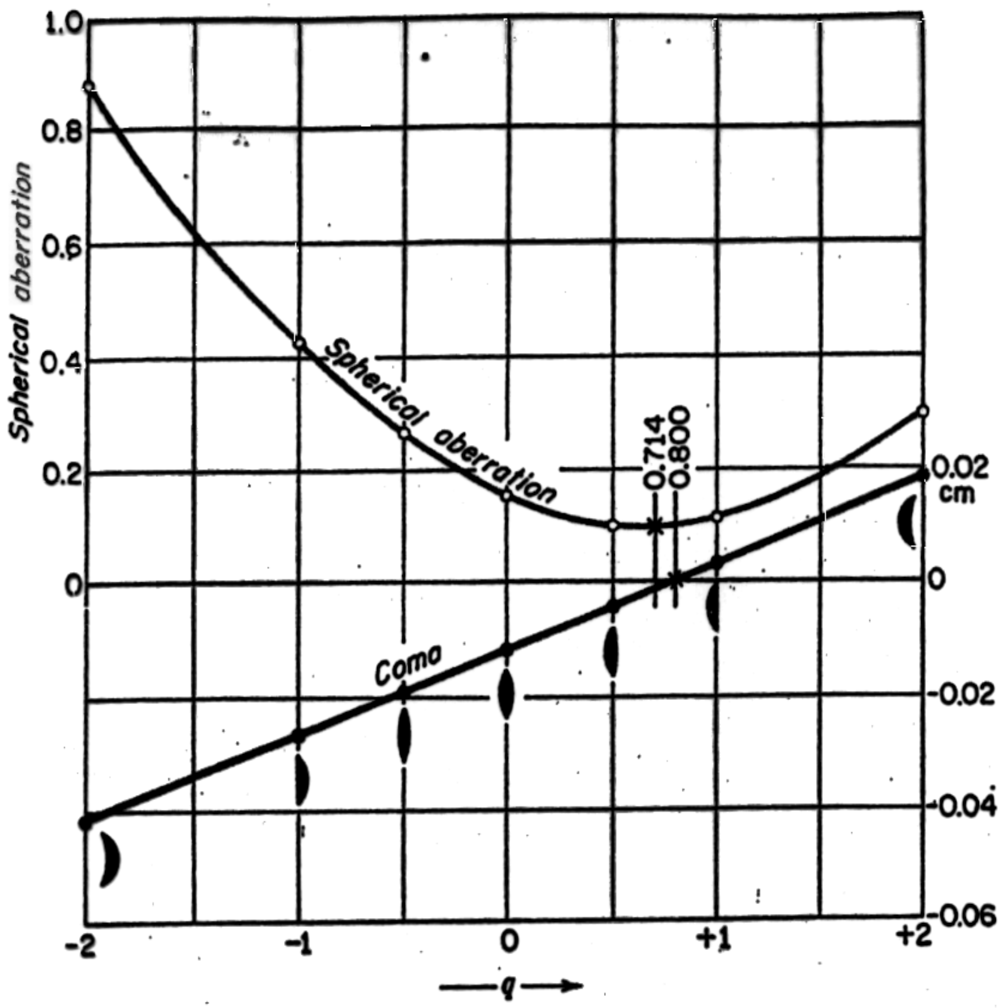

FIGURE 9L
Graphs comparing coma with longitudinal spherical aberration for a series of lenses having different shapes.

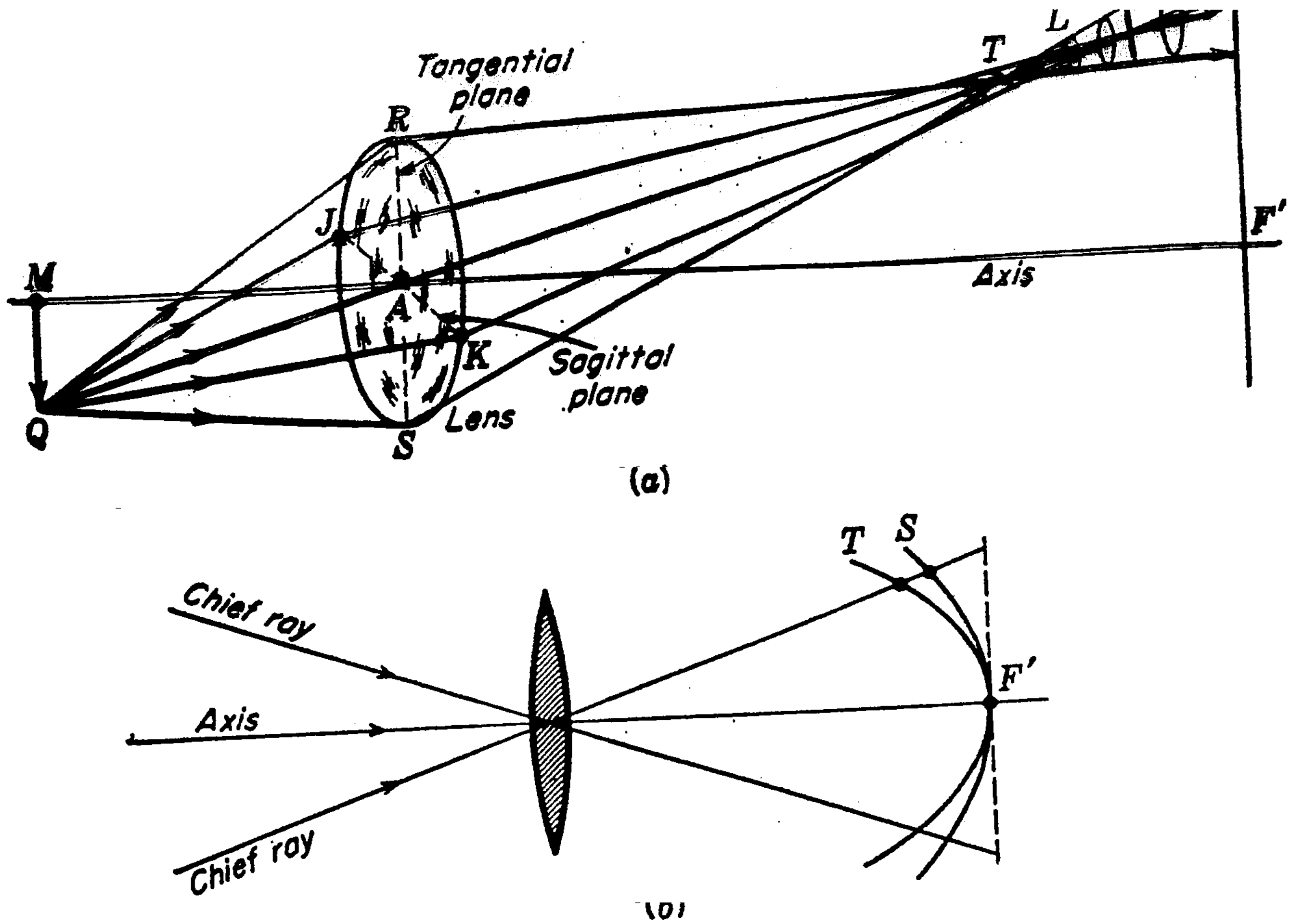

FIGURE 9P
(a) Perspective diagram showing the two focal lines which constitute the image

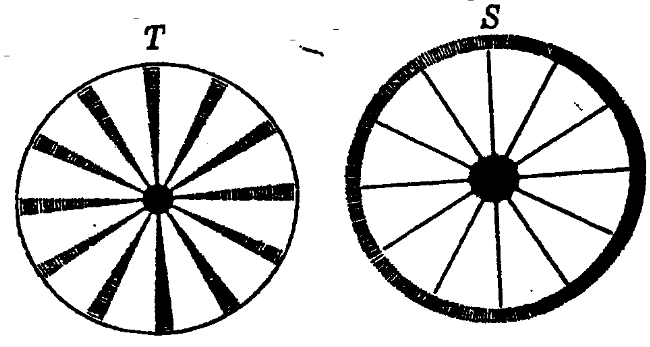

FIGURE 9Q
Astigmatic images of a spoked wheel.

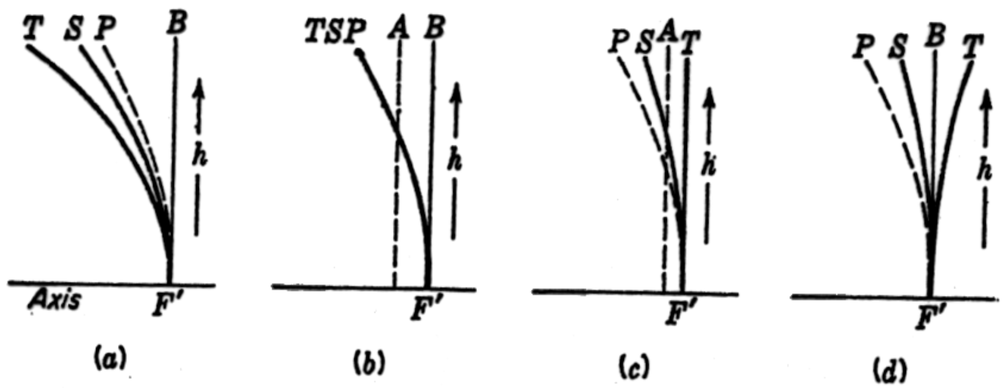

FIGURE 9R
Diagrams showing the astigmatic surfaces *T* and *S* in relation to the fixed Petzval surface *P* as the spacing between lenses (or between lens and stop) is changed.

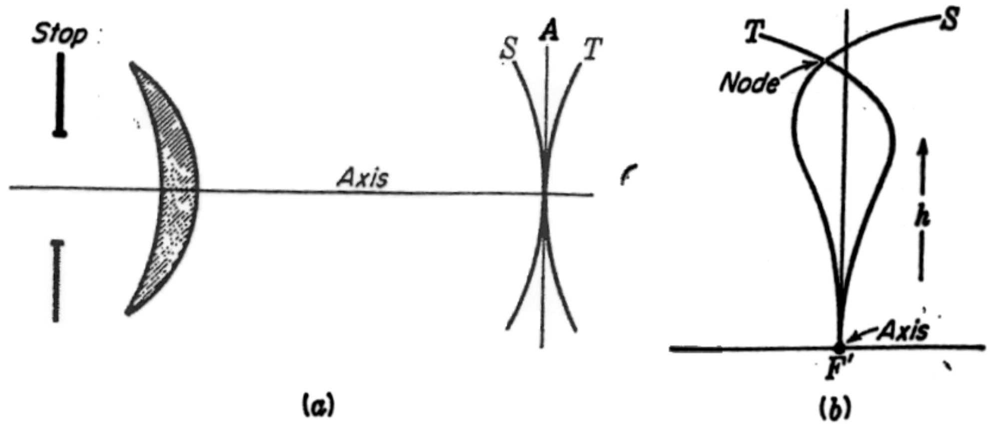

FIGURE 9S
(*a*) A properly located stop may be used to reduce field curvature. (*b*) Astigmatic surfaces for an anastigmat camera lens.

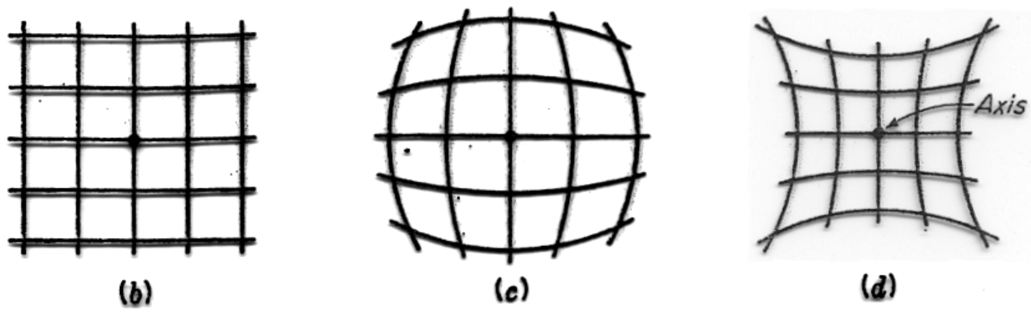

FIGURE 9T
(*a*) A pinhole camera shows no distortion. Images of a rectangular object screen shown with (*b*) no distortion, (*c*) barrel distortion, and (*d*) pincushion distortion.

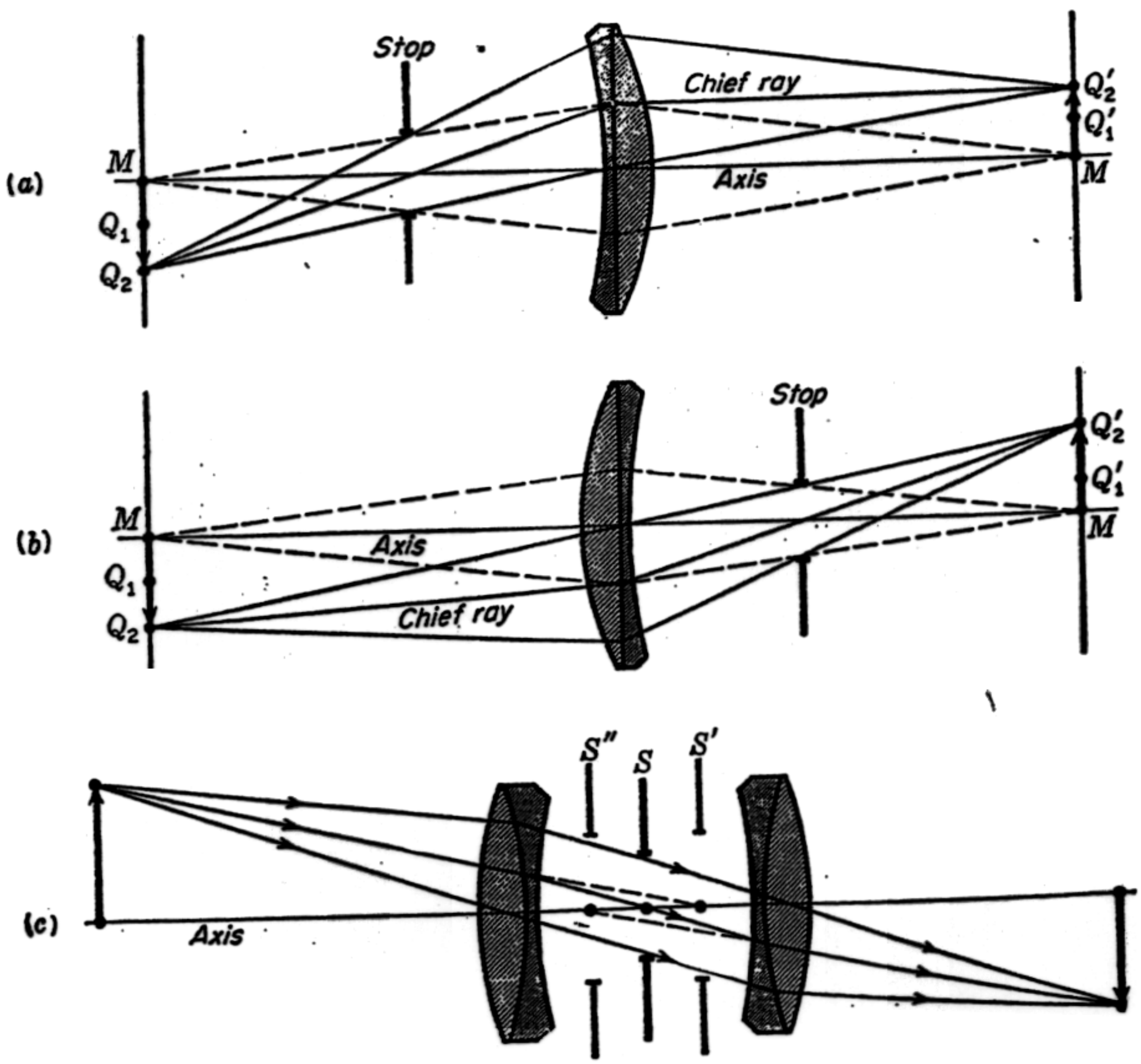

FIGURE 9U
(*a*) A stop in front of a lens giving rise to barrel distortion. (*b*) A stop behind a lens giving rise to pincushion distortion. (*c*) A symmetrical doublet with a stop between is relatively free of distortion.